THERMAL AND FIELD ENHANCED PHOTOEMISSION: COMPARISON OF THEORY TO EXPERIMENT

K. L. Jensen, Naval Research Laboratory, Washington DC, USA
D. W. Feldman, N. Moody, D. Demske, P. G. O'Shea, U. of Maryland, College Park, MD, USA

Abstract

Photocathodes are a critical component of high-gain FEL's and the analysis of their emission is complex. We have developed a time-dependent model accounting for the effects of laser heating and thermal propagation on photoemission. It accounts for surface conditions (coating, field enhancement, reflectivity), laser parameters (duration, intensity, wavelength), and material characteristics (reflectivity, laser penetration depth, scattering rates) to predict current distribution and quantum efficiency. The photoemission and quantum efficiency from metals and, in particular, dispenser photocathodes, is evaluated: the later introduces complications such as coverage non-uniformity and field enhancement.

INTRODUCTION

Photoinjectors are important electron sources for Free Electron Lasers (FEL's) due to the high quality electron beams that can be achieved, and may impact synchrotron light sources, high energy linear colliders, X-ray sources, and other applications [1-4] and in particular, Naval shipboard defense systems [5]. Photo injector concepts share a drive laser (which produces short bunches of photons) and photocathode (which converts the photon bunch into short bunches of electrons). The Quantum Efficiency, emittance generated at the cathode, cathode lifetime, survivability, emission promptness and uniformity are all issues. Metallic photocathodes are rugged and have fast response times (which allows for pulse shaping), but they have low QE and require incident UV light [6]. Direct band-gap p-type semiconductors (alkali antimonides and alkali tellurides [7-8], and bulk III-V with Cesium and oxidant [9]) are the highest QE photocathodes available and operate at longer wavelengths, but they are chemically reactive and easily poisoned by, e.g., H_20 and CO_2, damaged by back ion bombardment [10], and (for NEA III-V photocathodes) insufficiently responsive for pulse shaping in an rf injector due to their long emission time (> 40 ps for GaAs).

The ideal photocathode will have a high QE at the longest possible wavelength, be capable of *in situ* repair or rehabilitation, and demonstrate good lifetime. To meet the particular needs of a megawatt (MW) class FEL, it must produce 1 nC of charge in a 10-50 ps pulse every nanosecond (ns) (100 A peak and 1 A average current) in applied fields of 10-50 MV/m and background pressures of 0.01 mTorr – and to do so for several seconds. Such a cathode is presently unavailable, and even if it were, the ability to predict its performance and the beam it generates lacks adequate emission models. Dispenser cathodes have shown to have promise as photoemitters [11,12]. They consist of a work function coating diffusing out from a porous metal base and their operation has been extensively investigated. While dispenser cathodes are the focus of our program to develop rugged photocathodes, the theory and modeling developed to describe them have wider application

In this work, we characterize various dispenser cathodes and implement models of time-dependent and spatially varying laser interactions with various materials, in which an incident laser heats the electron gas within the metal and which subsequently equilibrates with the background lattice, and use those models to examine tungsten-based dispenser photocathodes and simple metals. The present work is an integral component in the execution of the agenda to qualify dispenser photocathodes and develop a suite of simulation tools that can characterize and predicatively estimate their performance.

CURRENT AND QUANTUM EFFICIENCY

Photoemitted current is the product of several factors: (*i*) the charge of the electron q; (*ii*) the amount of incident light absorbed (1-R), where R is the reflectivity; (*iii*) the number of incident photons; (*iv*) the probability that an electron has an energy greater than the barrier height following its absorption of a photon of frequency f; and (*v*) the probability that the electron migrates to the surface without suffering a scattering event. Using the Richardson approximation, the probability of (*iv*) can be expressed as a ratio of Fowler functions $U(x)$ defined by

$$U(x) = \int_{-\infty}^{x} \ln\left(1+e^{y}\right) dy \qquad [1]$$

The probability of emission is then $U[\beta(\phi-hf)]/U[\beta\mu]$, where $\beta = 1/k_B T_e$, k_B is Boltzmann's constant, T_e is temperature, and ϕ is the barrier height above the chemical potential μ. The current density is then

$$J_\lambda\left(T_e, F, \Phi\right) = f_\lambda \frac{q}{\hbar\omega}\left(1-R\right) I_\lambda(t) \frac{U\left[\beta\left(\hbar\omega-\phi\right)\right]}{U\left[\beta\mu\right]} \qquad [2]$$

to which must be added the thermal current given by Richardson's Equation, $J_{RLD} = A\ T^2 \exp(-\beta\phi)$. From the definition of quantum efficiency (QE) as the ratio of the total emitted electrons with total incident (not absorbed) photons, it follows that

$$QE = \frac{\hbar\omega}{q} \frac{\int_{-\infty}^{\infty}\int_{0}^{\infty} J\left[F(\rho), T(\rho,t)\right] 2\pi\rho d\,\rho dt}{\int_{-\infty}^{\infty}\int_{0}^{\infty} I(\rho,t) 2\pi\rho d\,\rho dt} \qquad [3]$$

where F is the spatially varying applied field, T is the time-dependent and spatially varying electron temperature, ρ is a cylindrical coordinate, and t is time.

We shall neglect the contribution of tunneling current (though we have treated it elsewhere [13]), even though for machined dispenser cathodes, sporadic field enhancement factors can be large and contribute to dark current due to field emission [14]. Dispenser cathodes have non-uniform low work-function (Φ) coatings. Consequently, Φ is spatially varying, making the evaluation of Eq. [3], if not impossible, then very difficult. We use instead a patch model

$$\int J(x,y)\,dA = \sum_{i,j}\int_{patch} J(x,y)\,dA_{i,j} \qquad [4]$$

where A_{ij} is the area of the i,j^{th} patch on a grid, and assume that all patches are equivalent. The patch encompasses one pore from which Barium (or other coatings) dispense, and the coverage θ is assumed to vary radially from the pore like $\theta(\rho) = \{1 + \exp[(\rho-\rho_o)/\Delta\rho]\}^{-1}$. $\Phi(\theta)$ is evaluated from our version of Gyftopolous-Levine theory

$$\Phi(\theta) = \Phi_f + (\Phi_W - \Phi_f)[1 - G(\theta)]H(\theta)$$
$$H(\theta) = (1-\theta)^2(1+2\theta) \qquad [5]$$

where G is a function of atomic and covalent radii of the bulk (tungsten) and coverage (barium) atoms, and Φ_f is the work function of a monolayer of coverage [15, 16]. the performance of Eq. [5] is shown in Figure 1.

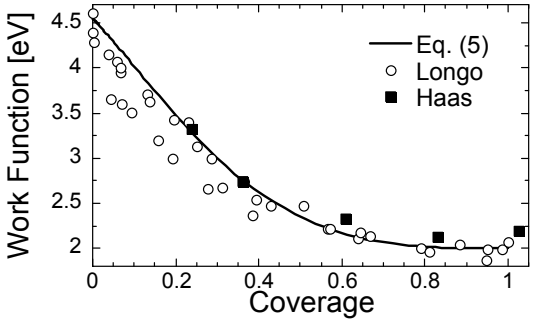

Figure 1: Work function dependence on coverage compared to experimental data [17,18] for BaO on W.

TIME DEPENDENT ELECTRON AND LATTICE TEMPERATURE EVALUATION

The Heat Diffusion Equations

Laser illumination and temperature variation for various metals have been considered extensively in the literature [19-23]. Here, we discuss the time dependent extension of procedures introduced in Ref. [5] insofar is it diverges from the steady state models therein. For those electrons not directly photoemitted, laser energy is transferred into electronic excitations. The hot electrons then come into equilibrium with other electrons via electron-electron scattering. The hot thermal Fermi-Dirac distribution comes into thermal equilibrium with the lattice via electron-phonon scattering. For laser pulse durations longer than the relaxation times associated with these processes, photons will encounter a heated electron distribution that, depending on intensity, can have temperatures significantly in excess of the bulk temperature, leading to complicating effects. In metals, a hot electron gas requires a fraction of a nanosecond to relax to its equilibrium state. The differential equations to determine electron and lattice temperatures are

$$C_e\frac{\partial}{\partial t}T_e = \frac{\partial}{\partial z}\left(\kappa\frac{\partial}{\partial z}T_e\right) - g(T_e - T_i) + G(z,t)$$
$$C_i\frac{\partial}{\partial t}T_i = g(T_e - T_i) \qquad [6]$$

where: C_e, C_i, and κ are the temperature-dependent specific heats and thermal conductivity; $G(z,t)$ governs the incident laser; and g governs the transfer of electron energy to the lattice (the notation follows Papadogiannis, *et al.*). Each term in Eq. [6] is replete with complications. The laser term is given by

$$G(z,t) = (1 - R(\theta_i))I(t)\left(\frac{e^{-z/\delta}}{\delta}\right)\left[1 - \frac{U[\beta(\hbar\omega - \phi)]}{U[\beta\mu]}\right] \qquad [7]$$

where R is the reflectivity, θ_i the incidence angle, I the laser intensity, and δ is the penetration depth. R and δ are functions of wavelength and evaluated from tabulated data of the index of refraction $n(E)$ and damping constant $k(E)$, as a function of photon energy E, from which R and δ follow [24], as in Figure 2. For normal incidence (θ_i = 0), R reduces to $R = [(n-1)^2+k^2]/[(n+1)^2+k^2]$.

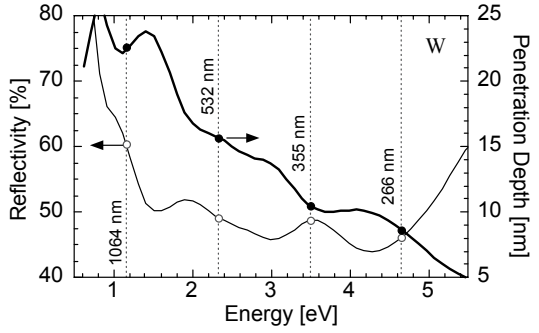

Figure 2: Reflectivity and penetration depth as a function of photon energy for normal incidence on tungsten.

The derivation of the specific heat terms for electrons and phonons follows standard solid state formulae, approximated from their exact forms in order to provide a reasonable fit over the temperature ranges we desire for numerical expedience. In these calculations, the electron number density, Debye temperature, atoms per unit cell, and sound velocity determine C_e and C_i and are calculated via a library of data for various bulk and coating materials (*e.g.,* the number of atoms per unit cell, the sound velocity, and the Debye temperature for tungsten is 0.2697, 5220 m/s, and 400 K, respectively). At high(er) temperatures, C_e and C_i are linear and constant in electron and lattice temperature, respectively.

The coefficient g and the thermal conductivity κ depend on electron-electron and electron-lattice relaxation time τ (see [5] and references therein), though now the joint relaxation time can depend on differeing T_e and T_i, as in

$$\tau\left(T_e,T_i\right)^{-1}=\tau_{ee}\left(T_e\right)^{-1}+\tau_{ph}\left(T_i\right)^{-1}$$
$$\tau_{ee}\left(T_e\right)=\frac{\hbar\mu}{A_o}\left(\frac{1}{k_BT_e}\right)^2;\tau_{ph}\left(T_i\right)=\frac{\hbar}{2\pi\lambda_o}\left(\frac{1}{k_BT_i}\right) \quad [8]$$

Thermal conductivity is an experimentally tabulated property as a function of temperature. Consequently, the dimensionless constants A_o and λ_o can be extrapolated from it and Eq. [8] – which is adequate for a many metals from room temperature to high temperatures – though tungsten contains behavior which departs from that approximation around room temprature. For dispenser cathodes, λ_o is allowed to vary slightly, reflecting that the base is an odd compilation of tungsten pellets and impregnants, and therefore not bulk material.

After an electron absorbs a photon, it is assumed to travel in a random direction and possibly suffer one or more collisions on its journey to the surface. Let any collision terminate the probability of emission (an overzealous assumption). The factor f_λ is then approximated by $f_\lambda\left(m\delta/\hbar k_o\tau\right)$ [13] where $\hbar$ is Planck's constant over 2π, k_o is the wave vector equivalent of the energy height of the barrier above the conduction band minimum, and the $f_\lambda(x)$ is defined by

$$f_\lambda\left(x\right)=\frac{1}{\pi}\int_0^{\pi/2}\frac{\cos\left(s\right)}{\cos\left(s\right)+x}ds \quad [9]$$

EXPERIMENTAL RESULTS AND COMPARISONS TO THEORY

Dispenser Cathode Quantum Efficiency

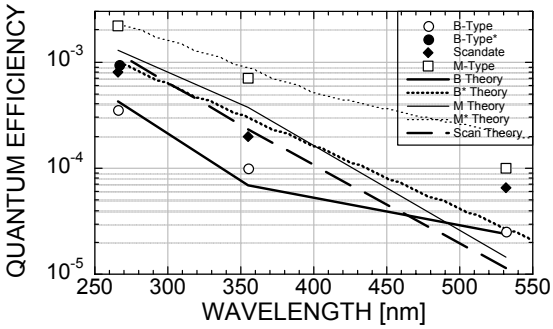

Figure 3: QE of Dispenser photocathodes. Lines are theory, points are exp. data. See text for details.

We have extensively described the experimental apparatus and conditions under which measurements were taken in previous works [5, 12]. Here, we report on intensity and field variation of emitted charge, the wavelength dependence of the quantum efficiency of both dispenser cathodes and simple metals, and their comparisons with predictions of the time dependent laser heating and photoemission modeling described above.

Theory and experimental data points for dispenser photocathodes are shown in Figure 3. The correspondence is as follows: white circle = B-type (Ref. [11]). Black circle = B-type (Ref. [25].) Black diamond: scandate. Thick solid & short dashed line: theory using Ref. [11] and Ref. [25] parameters, respectively. Thin solid and short dashed line: M-type using actual and extrapolated fields of 1.7 MV/m and 50 MV/m (a field typical of the operational environment of a MW-class FEL injector), respectively for 4.5 ns pulses and bulk temperature of 723 K. Thick long-dashed line: Scandate theory. The M-type cathodes have a coating of Osmium on the surface. It is seen that with the rather generic parameters used, theory underestimates the experimental performance of the M-type cathode by less than a factor of 2 at shorter wavelengths; at longer wavelengths, where the photon energy is comparable to the barrier height, the differences are more pronounced: a possibility is that tunneling effects may contribute more for such work functions and conditions. Both B and M-type performance vary depending on conditioning and processing of the cathode. For the scandate theory line, a smaller value of ρ_o was used in the patch model than for the field and intensity analysis (below), resulting in a smaller coverage factor of $\langle\theta\rangle = 12\%$.

Dispenser Cathode performance

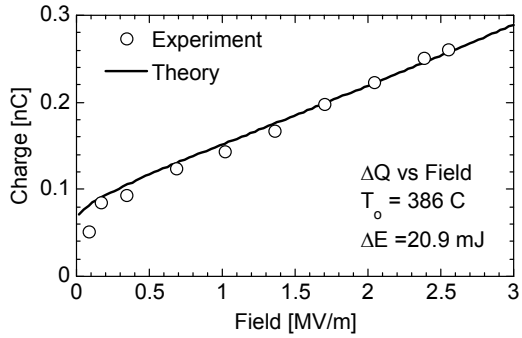

Figure 4: Emitted charge *vs.* field for scandate cathode.

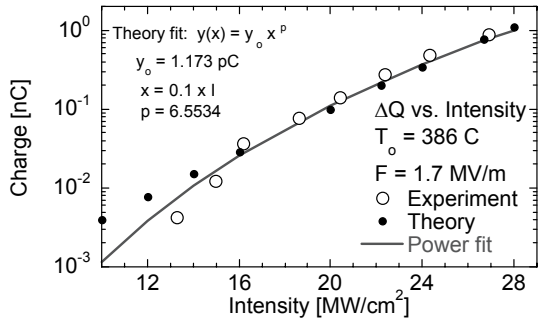

Figure 5: Same as Fig. 4, but for variation in intensity.

The modeling of Scandate dispenser cathodes using standard dispenser models is complicated by the barrier lowering mechanism, which may be more semiconductor-like band bending than patchy surface [26]. The simulations of QE for the scandate cathodes used the input data used to model the field and intensity variation: while these measurements occurred on separate occasions

and illuminating different regions of the cathode, and required $\langle\theta\rangle$=45%, and a field enhancement of 4.46, we did not separately adjust parameters when modeling intensity, using the same parameters as used for field. The field variation is shown in Figure 4 using a 4.5 ns FWHM pulse and the first harmonic (1064 nm) wavelength. Using the input data of Figure 4, the intensity dependence was calculated and compared to experiment, as shown in Figure 5.

Quantum Efficiency of Metals

Dispenser cathodes, owing to their odd constitution, induce complications that bulk metals do not. We therefore sought to compare the simulation code with quantum efficiencies for various metals determined by Srinivasan-Rao, *et al.* [27], for which gold, magnesium, and copper were selected.

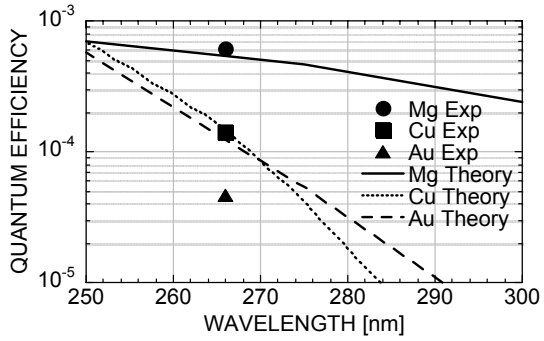

Figure 6: QE for Au, Cu, and Mg using theoretical model compared to 266 nm data from Ref. [26].

In Figure 6, all parameters were based on bulk values obtained from CRC and AIP Handbook tables, and operating conditions and parameters cited in Ref. [26]. The only adjustable parameter was field enhancement, which was set to 1.0, 2.5, and 7.0 for Au, Cu, and Mg, respectively, a range no different than that found for the dispenser cathode simulations. The performance of the model for Mg and Cu was good. The modeling performs less satisfactorily for Au, but nevertheless reasonable.

SUMMARY

We have reported on the characterization of several dispenser cathodes, and have confirmed their potentially attractive features as photoemitters, *e.g.,* low work function and high quantum efficiency, rejuvenation capabilities, and wavelength characteristics. Models were developed to simulate and predict their performance and performed well for our data as well as results for dispenser and metal photocathodes reported in the literature.

Acknowledgements

We gratefully acknowledge funding provided by the *Joint Technology Office* and the *Office of Naval Research.*

REFERENCES

[1] P. G. O'Shea, H. Freund, *Science* **292**, 1853 (2001).
[2] T. Srinivasan-Rao, J. Schill, I. Ben Zvi, M. Woodle, *Rev. Sci. Instrum*. **69**, 2292 (1998)
[3] C. Travier, G. Devanz, B. Leblond, B. Mouton, *Nucl. Inst. Meth. Phys. Res.* **A393**, 451 (1997).
[4] C. Hernandez Garcia, C. A. Brau, *Nucl. Inst. Meth. Phys*. **A483**, 273 (2002).
[5] K. L. Jensen, D. W. Feldman, M. Virgo, P. G. O'Shea, *Phys. Rev. Spec. Top.* **AB6**, 083501 (2003).
[6] J. A. Nation, L. Schächter, F. M. Mako, L. K. Len, W. Peter, C.-M. Tang, T. Srinivasan-Rao, *Proceedings of the IEEE* **87**, 865 (1999).
[7] W. E. Spicer, Phys. Rev. 112, 114 (1958); W. E. Spicer, A. Herrera-Gómez, SLAC-PUB-6306 & SLAC/SSRL-0042, Aug 1993.
[8] P. Michelato, *Nucl. Inst. Meth. Phys. Res*. **A393**, 455 (1997).
[9] T. Maruyama, R. Prepost, E. Garwin, C. K. Sinclair, B. Dunham, *Appl. Phys. Lett.* **55**, 1686 (1989)
[10] C. K. Sinclair, *Proc. 1999 Particle Accelerator Conf.,* (New York, IEEE, Piscataway, NJ, 1999) p 65.
[11] B. Leblond, *Nucl. Inst. Meth. Phys. Res.* **A317**, 365 (1992).
[12] K. L. Jensen, D. W. Feldman, P. G. O'Shea (*submitted for publication in Appl. Phys. Lett.*).
[13] K. L. Jensen, D. W. Feldman, P. G. O'Shea, *Proc. Of the Int'l. Vacuum Nanoelectronics Conference*, (Cambridge MA, July, 2004).
[14] A. H. Lumpkin, *Conference Record of the 1991 IEEE Particle Accelerator Conference,* Vol 3, 1967 (1991).
[15] J. D. Levine, E. P. Gyftopolous, *Surf. Sci.* **1**, 171 (1964); *ibid*, 225 (1964); *ibid*, 349 (1964).
[16] K. L. Jensen, Y. Y. Lau, B. Levush, *IEEE Trans. Plas. Sci.* **28**, 772 (2000).
[17] R. T. Longo, E. A. Adler, L. R.Falce, *Tech. Dig. of the IEDM*, 318 (1984).
[18] G. A. Haas, A. Shih, C. R. K. Marrian, *Appl. Surf. Sci.* **16**, 139 (1983).
[19] E. M. Logothetis, P. L. Hartman, *Phys. Rev.* **187**, 460 (1969).
[20] J. H. Bechtel, *J. Appl. Phys.* **46**, 1585 (1975).
[21] D. M. Riffe, X. Y. Wang, M. C. Downer, D. L. Fisher, T. Tajima, J. L. Erskine, R. M. More, *J. Opt. Soc. Am.* **B10**, 1424 (1993).
[22] X. Y. Wang, D. M. Riffe, Y.-S. Lee, M. C. Downer, *Phys. Rev.* **B50**, 8016 (1994).
[23] N. A. Papadogiannis, S. D. Moustaïzis, and J. P. Girardeau-Montaut, *J. Phys. D: Appl. Phys*. **30**, 2389 (1997); N. A. Papadogiannis, S. D. Moustaïzis, *J. Phys. D: Appl. Phys.* **34**, 2389 (2001).
[24] G. Haas, L. Hadley, "Chapter 6g", *AIP Handbook*, 3rd Ed, D. E. Gray (ed) (McGraw-Hill, New York, 1972).
[25] C. Travier, B. Leblond, M. Bernard, J. N. Cayla, P. Thomas, P. Georges, *Proc. Par. Accel. Conf.* (1995)
[26] J. Yater, A. Shih (NRL) (*private communication*).
[27] T. Srinivasan-Rao, J. Fischer, T. Tsang, *J. Appl. Phys.* **69**, 3291, (1990)